Electronic Supplementary Material (ESI) for Materials Horizons.
This journal is © The Royal Society of Chemistry 2019

Supplementary Information for:

Super-Soft Solvent-Free Bottlebrush Elastomers for Touch Sensing

Veronica G. Reynolds[†▽^], Sanjoy Mukherjee[‡▽^], Renxuan Xie[†▽], Adam E. Levi[+▽], Amalie Atassi[‖], Takumi Uchiyama[⊥], Hengbin Wang[▽], Michael L. Chabinyc[†▽*], Christopher M. Bates[†+§▽*]

[†]*Materials Department,* [‡]*Materials Research Laboratory,* [+]*Department of Chemistry and Biochemistry,* [§]*Department of Chemical Engineering, and* [▽]*Mitsubishi Chemical Center for Advanced Materials, University of California, Santa Barbara, California 93106, United States*

[‖]*Department of Materials Science and Engineering, University of Florida, Gainesville, Florida, United States*

[⊥]*Department of Materials Science and Engineering, Tokyo Institute of Technology, Tokyo, Japan*

[^]*These authors contributed equally*

Table of Contents

I. Synthesis

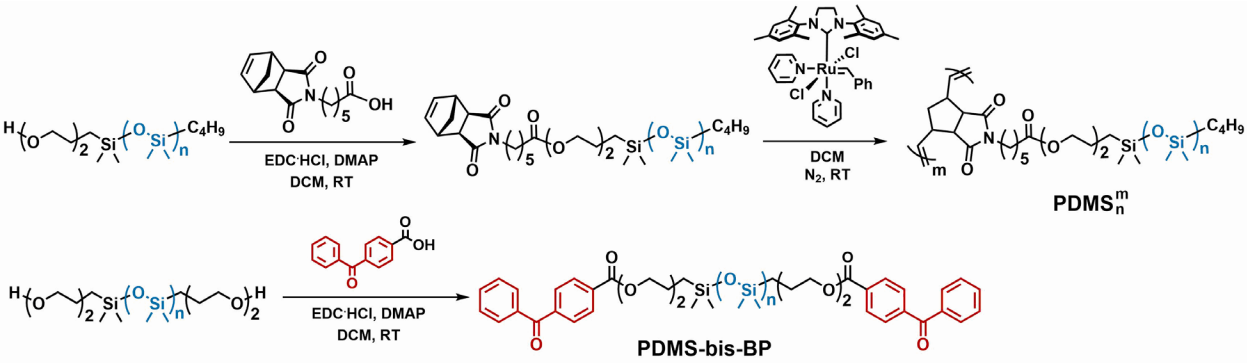

Scheme S1. Synthesis of PDMS bottlebrush polymers (top) and PDMS bis-benzophenone crosslinker (bottom).

Materials and Methods

N-(hexanoic acid)-*cis*-5-norbornene-*exo*-dicarboximide was prepared according to literature.[1] Grubbs' second-generation metathesis catalyst [$(H_2IMes)(PCy_3)(Cl)_2Ru{=}CHPh$] was generously provided by Materia. Grubbs' third-generation metathesis catalyst [$(H_2IMes)(pyr)_2(Cl)_2Ru{=}CHPh$] (G3) was prepared according to literature.[2] Methanol (Fisher Scientific — A412; purity >99.8%), dichloromethane (Fisher Scientific — D37, purity >99.5%), and ethyl vinyl ether (Fisher Scientific / ACROS Organics, AC119082500, purity >99%) were used as received. $CDCl_3$ (99.8%) was purchased from Cambridge Isotope Laboratories (DLM-7) and used as received. Bis(hydroxyalkyl)-terminated PDMS (Sigma — 481246), hydroxyalkyl-terminated PDMS (Gelest — MCR-C18), 4-benzoylbenzoic acid (Sigma — B12407, purity 99%), *N,N*-dimethylaminopyridine (Alfa Aesar, H51715, purity 99%) and EDC (Oakwood chemical-024810, purity 99%) were used as received.

Synthesis of PDMS-bis-BP Crosslinker

In a round-bottom flask, a mixture of 4-benzoylbenzoic acid (1.21 g, 5.36 mmol), bis(hydroxyalkyl)-terminated 5.6 kDa PDMS (10 g, 1.79 mmol), DMAP (109 mg, 0.9 mmol), and EDC•HCl (1.37 g, 7.14 mmol) in DCM (100 mL) was stirred for 24 hours. The reaction mixture was washed with dilute HCl (1 M) and repeatedly washed with water, followed by drying over anhydrous $MgSO_4$. The solution was passed through a plug of activated basic alumina and

evaporated to dryness to obtain the desired compound as a transparent colorless liquid. Yield: 5.75 g (53 %). ^{1}H NMR (600 MHz, Chloroform-*d*) δ: 8.18 (d, *J* = 8.2 Hz, 4H), 7.84 (d, *J* = 8.2 Hz, 4H), 7.81 (d, *J* = 8.1 Hz, 4H), 7.61 (t, *J* = 7.4 Hz, 2H), 7.50 (t, *J* = 7.7 Hz, 4H), 4.53 – 4.50 (m, 4H), 3.81 – 3.77 (m, 4H), 3.50 (t, *J* = 6.9 Hz, 4H), 1.64 (dd, *J* = 15.3, 8.0 Hz, 4H), 0.58 – 0.54 (m, 4H), 0.08 (s, 475H). ^{13}C NMR (151 MHz, Chloroform-*d*) δ: 195.88, 165.73, 141.33, 136.97, 133.25, 132.85, 130.05, 129.68, 129.57, 128.40, 74.15, 68.45, 64.58, 23.39, 14.10, 1.23, 1.12, 0.99, 0.74, 0.07.

Synthesis of PDMS Macromonomer

In a round-bottom flask, a mixture of mono-hydroxy 5 kDa PDMS (54.3 g, 10.9 mmol), *N*-(hexanoic acid)-*cis*-5-norbornene-*exo*-dicarboximide (7.53 g, 27.2 mmol), DMAP (663 mg, 5.43 mmol), and EDC•HCl (7.3 g, 38.0 mmol) in DCM (250 mL) was stirred for 48 hours. The reaction mixture was washed with dilute HCl (1 M) and repeatedly washed with water, followed by drying over anhydrous $MgSO_4$. The solution was passed through a plug of activated basic alumina and evaporated to dryness to obtain the desired compound as a transparent colorless liquid. Yield: 50.1 g (88%). ^{1}H NMR (600 MHz, Chloroform-*d*) δ: 6.28 (t, *J* = 1.8 Hz, 2H), 4.22 – 4.19 (m, 2H), 3.48 – 3.44 (m, 2H), 3.42 (t, *J* = 7.1 Hz, 2H), 3.27 (s, 2H), 2.67 (s, 2H), 2.33 (t, *J* = 7.5 Hz, 2H), 1.62 (ddt, *J* = 34.6, 15.2, 7.6 Hz, 8H), 1.51 (d, *J* = 9.8 Hz, 1H), 1.36 – 1.26 (m, 6H), 1.21 (d, *J* = 9.9 Hz, 1H), 0.88 (t, *J* = 7.0 Hz, 4H), 0.57 – 0.49 (m, 4H), 0.07 (s, 278H).

Synthesis of Bottlebrush Polymers:

Polymerizations of the macromonomers using G3 catalyst were performed in dilute solutions of the macromonomer (0.02 g mL^{-1}) in dry DCM. Catalyst was injected as a dilute solution in dry DCM (e.g., 500 µL of 0.029 g mL^{-1}) and the equivalents relative to macromonomer were varied depending on the target backbone degree of polymerization (N_{BB}). Polymerizations were terminated using ethyl vinyl ether after 6 hours. The resulting reaction mixtures were concentrated *in vacuo* and the polymers were precipitated in methanol. After two more consecutive precipitations of the polymers in methanol, the bottlebrush polymers were collected and dried under vacuum.

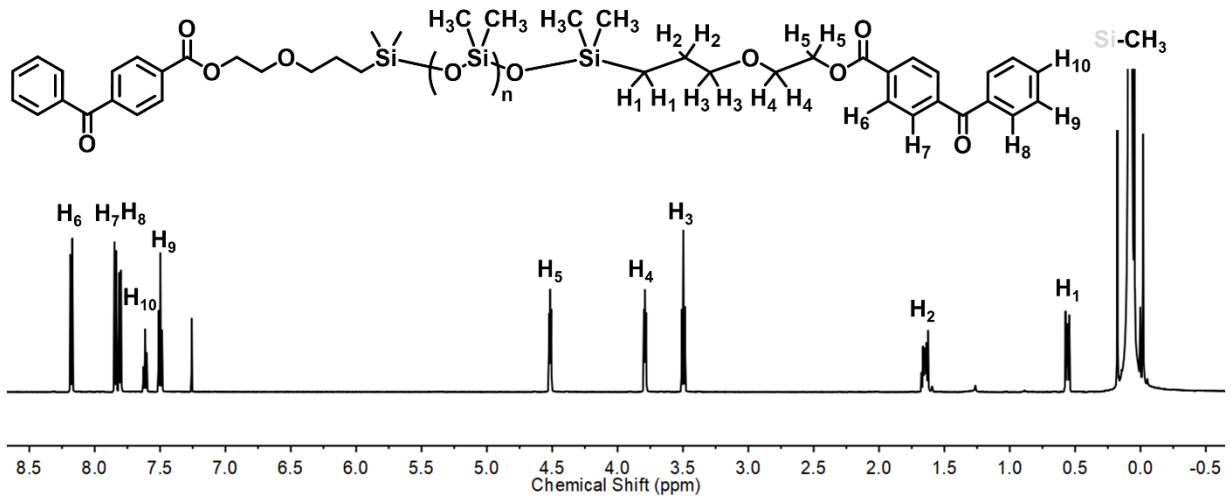

Figure S1. ^{1}H NMR of PDMS-bis-BP in $CDCl_3$.

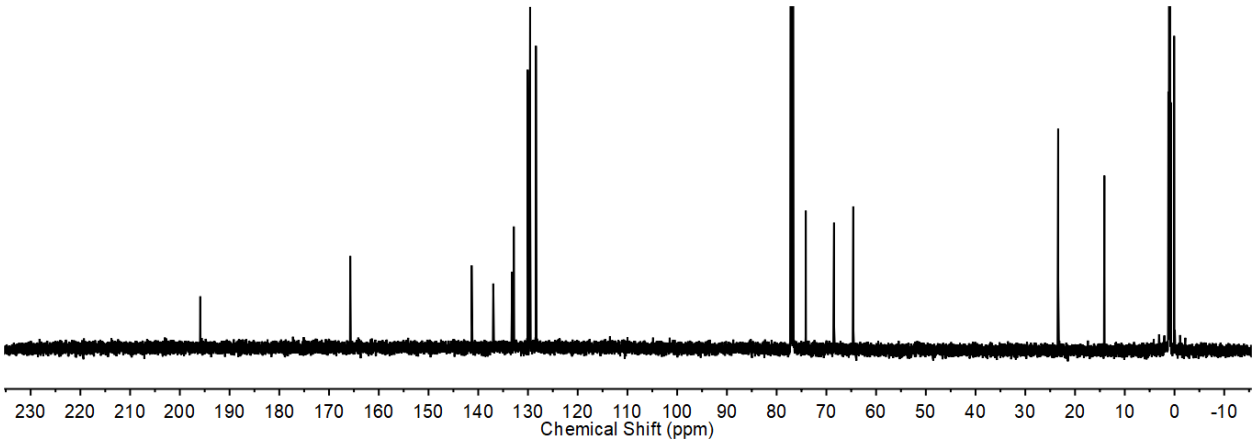

Figure S2. ^{13}C NMR of PDMS-bis-BP in $CDCl_3$.

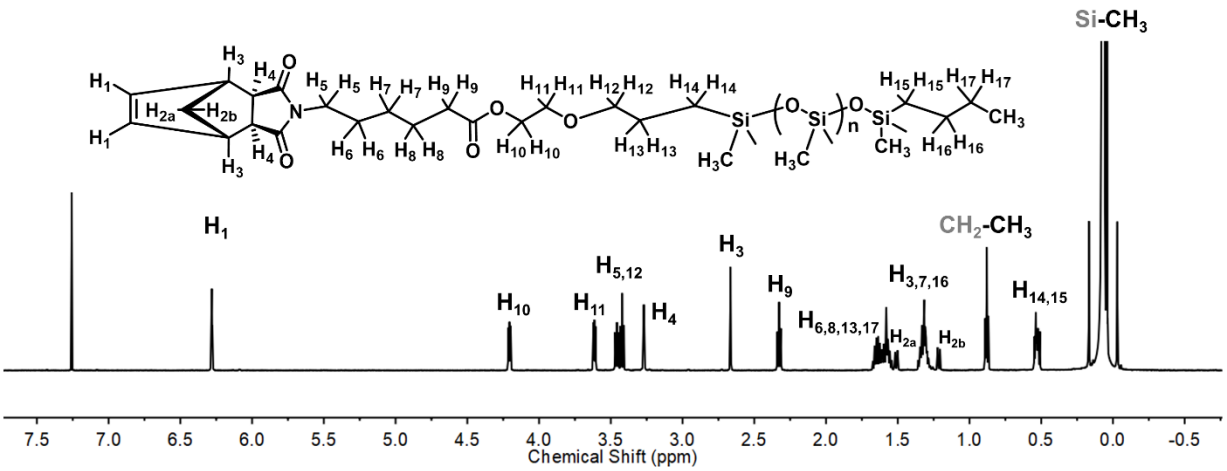

Figure S3. ^{1}H NMR of PDMS macromonomer in $CDCl_3$.

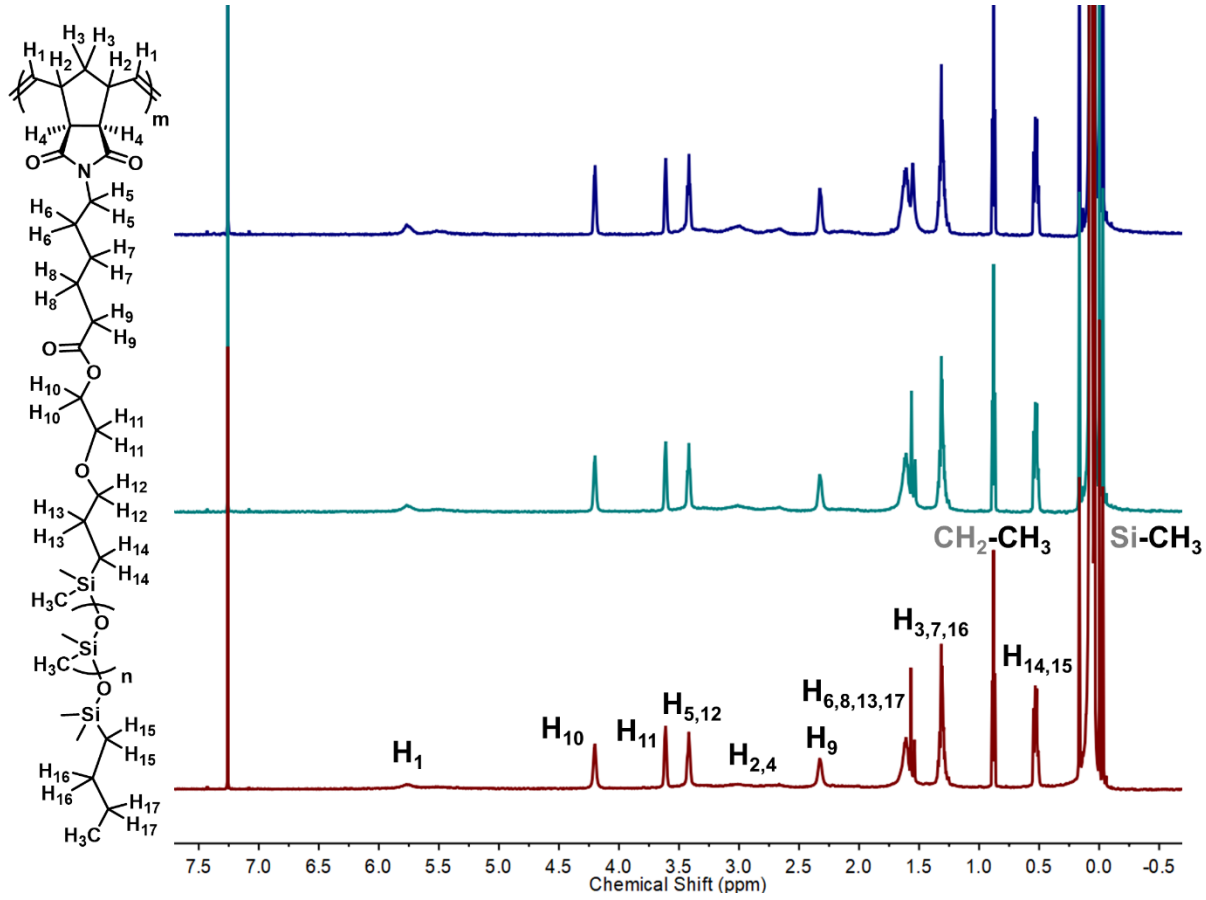

Figure S4. ^{1}H NMRs of the bottlebrush polymers in $CDCl_3$. From top to bottom: $PDMS_{68}^{20}$ (navy), $PDMS_{68}^{99}$ (teal), and $PDMS_{68}^{235}$ (maroon).

Size exclusion chromatography (SEC) was performed on a Waters Alliance HPLC System 2695 Separation Module equipped with two Agilent PLgel MiniMixed-D bed columns and multi-angle light scattering (Wyatt DAWN HELEOS-II, 663 nm laser light) and differential refractive index (Wyatt Optilab rEX) detectors. The absolute molar mass and molar mass distribution of PDMS bottlebrush polymers was measured in tetrahydrofuran (THF) at 30 ºC. Polymers were first dissolved in THF overnight with known and dilute concentrations (≤4.0 mg/mL) and then filtered through a 0.45 µm PTFE filter. The differential refractive index increment (dn/dc) was calculated by integrating the refractive index signal assuming 100% mass recovery as shown in Table S1. Although the values of dn/dc are very small (≈0.01 mL/g), the bottlebrush polymer molecular weights are still high enough to provide sufficient scattering signal in dilute solution. The number-average molar mass (M_n), molar mass dispersity (M_w/M_n), and the z-average radius of gyration ($R_{g,z}$) were determined by constructing a Zimm plot for each slice of the elution profile in Figure S5; the data are summarized in Table S1.

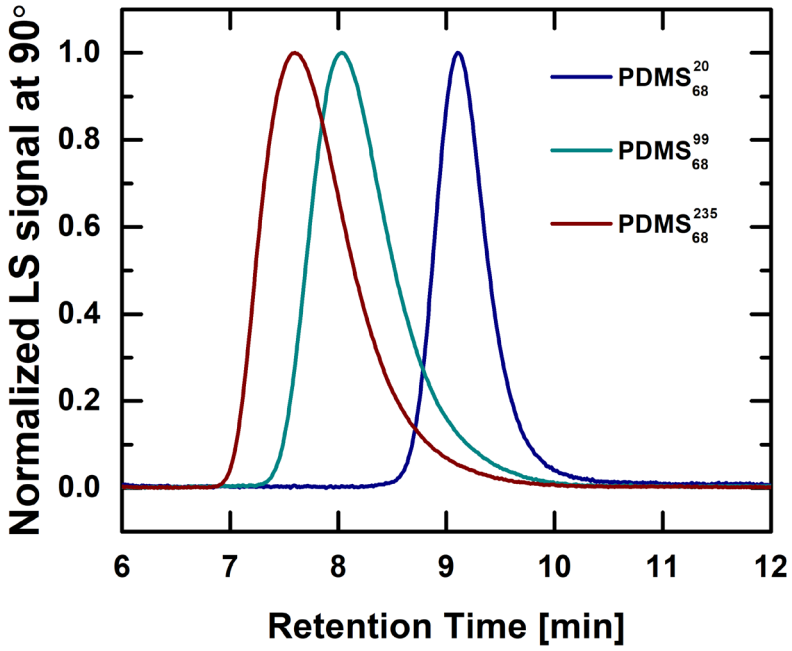

Figure S5. SEC profiles (light-scattering signal at 90°) of the bottlebrush polymers in THF.

Table S1. Characterization of the bottlebrush polymers by SEC-MALS

Material	M_n (kDa)	M_w/M_n	dn/dc (mL/g)	$R_{g,z}$ [nm]
$PDMS_{68}^{20}$	110	1.4	0.0196	6.5 ± 4.1
$PDMS_{68}^{99}$	520	1.4	0.0137	17.8 ± 0.9
$PDMS_{68}^{235}$	1200	1.4	0.0106	28.1 ± 0.5

II. Rheology

To determine the network moduli of PDMS elastomers, PDMS/crosslinker mixtures were first crosslinked *in situ* in an AR-G2 rheometer (TA Instruments). A 20-mm-diameter parallel plate geometry with a sample thickness of 0.4 mm was used for all rheology measurements in this work. For Sylgard 184, the mixture was cured by heating the sample to 150 ºC for 30 mins using a Peltier plate. The frequency-dependent moduli are shown before and after this curing process in Figure S6. For photo-crosslinking PDMS bottlebrush polymers, a UV LED light source with a 365 nm wavelength and irradiance of 150 mW/cm^2 was used to cure the sample *in situ* through a UV-transparent quartz bottom plate. The curing process was monitored by tracking the time evolution of shear moduli from a viscoelastic liquid to fully crosslinked elastomer as shown in Figure 4a. When curing, a constant oscillatory frequency of 10 rad/s and strain amplitude of 0.01 were used.

After complete curing as indicated by a plateau in the storage modulus during light exposure, the frequency dependence of the shear moduli at 21 ºC was collected by both a small-amplitude oscillatory shear test and stress relaxation test. Specifically, Figures S7–S10 show the frequency sweep response between 100 and 0.01 rad/s with an oscillatory strain amplitude of 0.01, which is well within the linear region for $PDMS_{68}^{20}$-2, $PDMS_{68}^{20}$-4, $PDMS_{68}^{99}$-12, and $PDMS_{68}^{235}$-12. Due to the presence of slow relaxation in PDMS elastomers, a stress relaxation test with a step strain of 0.01 was also conducted to probe the long-time (or low-frequency) behavior and reach the plateau storage modulus faster. In the linear viscoelastic regime, the stress relaxation result should be equivalent to the oscillatory shear result. Thus, by fast Fourier transforming (FFT) the stress relaxation response from the time to the frequency domain,[1] its frequency response is extended to an even lower frequency value of 0.001 rad/s, where the plateau storage modulus starts

to appear. Finally, the equilibrium network modulus (G_0) is determined as the plateau storage modulus at the lowest experimentally measured frequency (i.e., $G_0 = G'(0.001\ \text{rad/s})$).

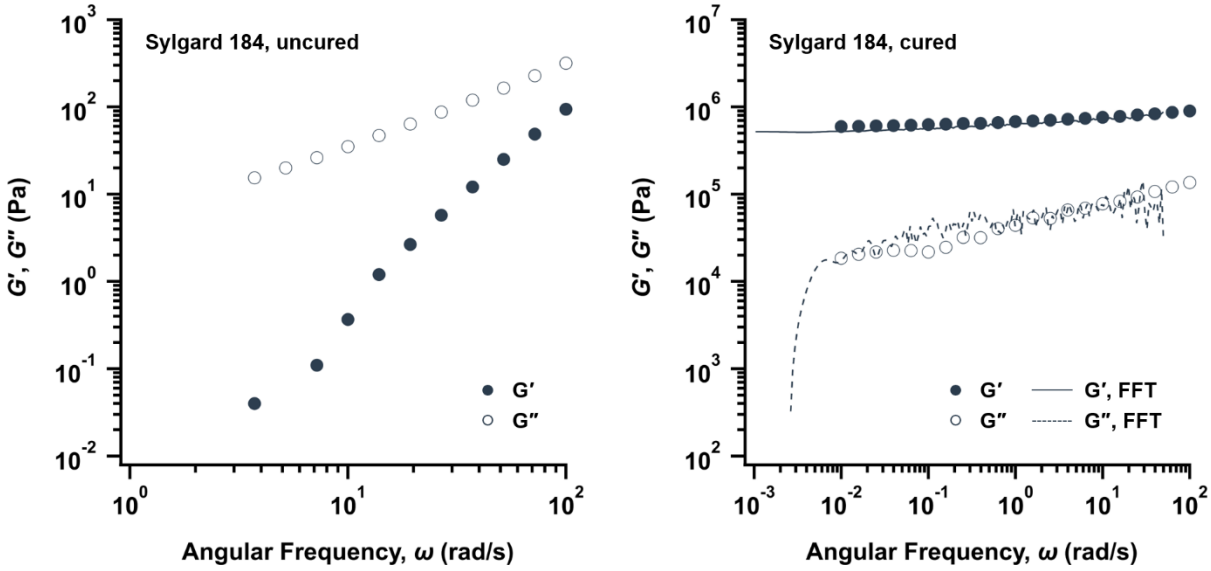

Figure S6. Frequency dependence of the shear moduli for uncured Sylgard 184 at 21 ºC with an oscillatory strain amplitude of 0.05 (left) and for crosslinked Sylgard 184 at 21 ºC with an oscillatory strain amplitude of 0.01 after curing at 150 ºC for 30 mins (right). The stress relaxation response with a step strain of 0.01 was fast Fourier transformed (FFT) to extend the frequency range to 0.001 rad/s.

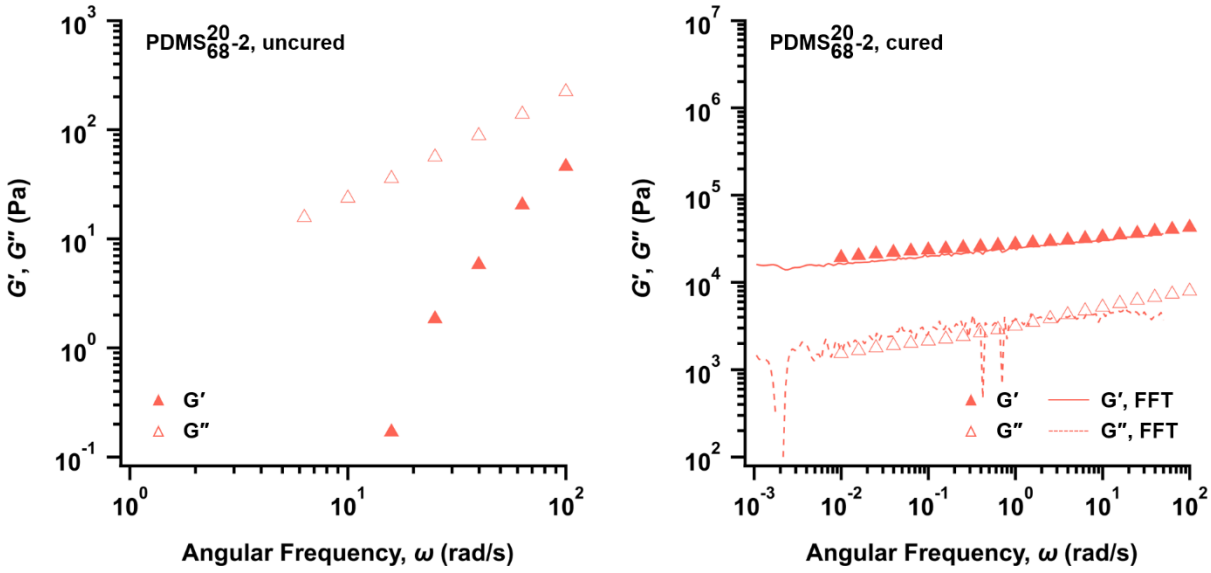

Figure S7. Frequency dependence of the shear moduli for uncured $PDMS_{68}^{20}$-2 at 21 ºC with an oscillatory strain amplitude of 0.05 (left) and for crosslinked $PDMS_{68}^{20}$-2 at 21 ºC with an oscillatory

strain amplitude of 0.01 after complete UV curing (right). The stress relaxation response with a step strain of 0.01 was fast Fourier transformed (FFT) to extend the frequency range to 0.001 rad/s.

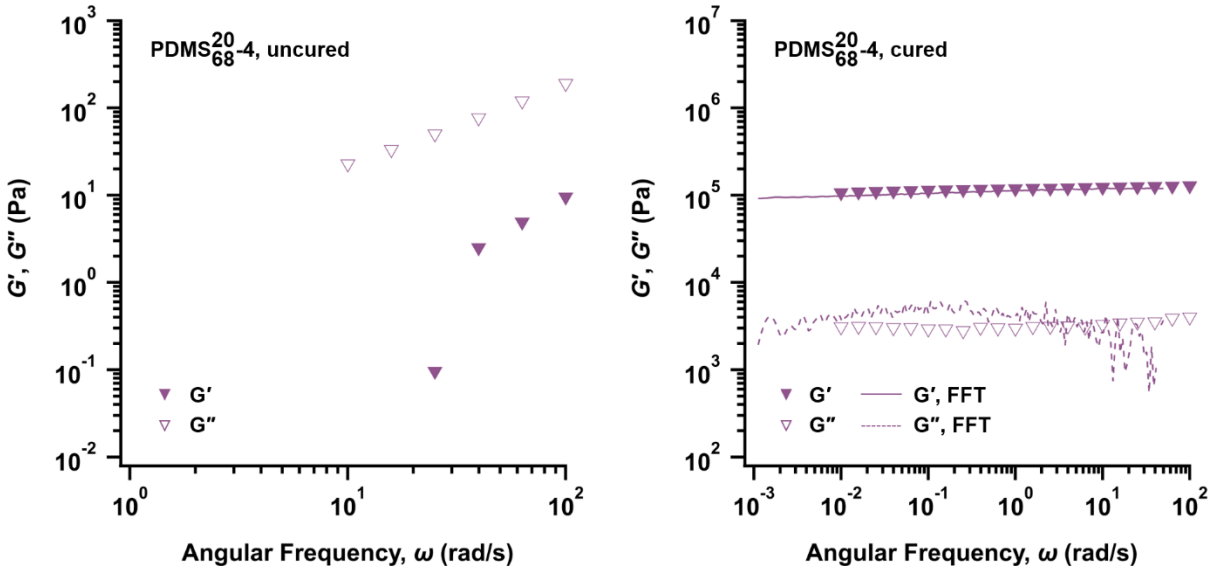

Figure S8. Frequency dependence of the shear moduli for uncured PDMS$_{68}^{20}$-4 at 21 ºC with an oscillatory strain amplitude of 0.05 (left) and for crosslinked PDMS$_{68}^{20}$-4 at 21 ºC with an oscillatory strain amplitude of 0.01 after complete UV curing (right). The stress relaxation response with a step strain of 0.01 was fast Fourier transformed (FFT) to extend the frequency range to 0.001 rad/s.

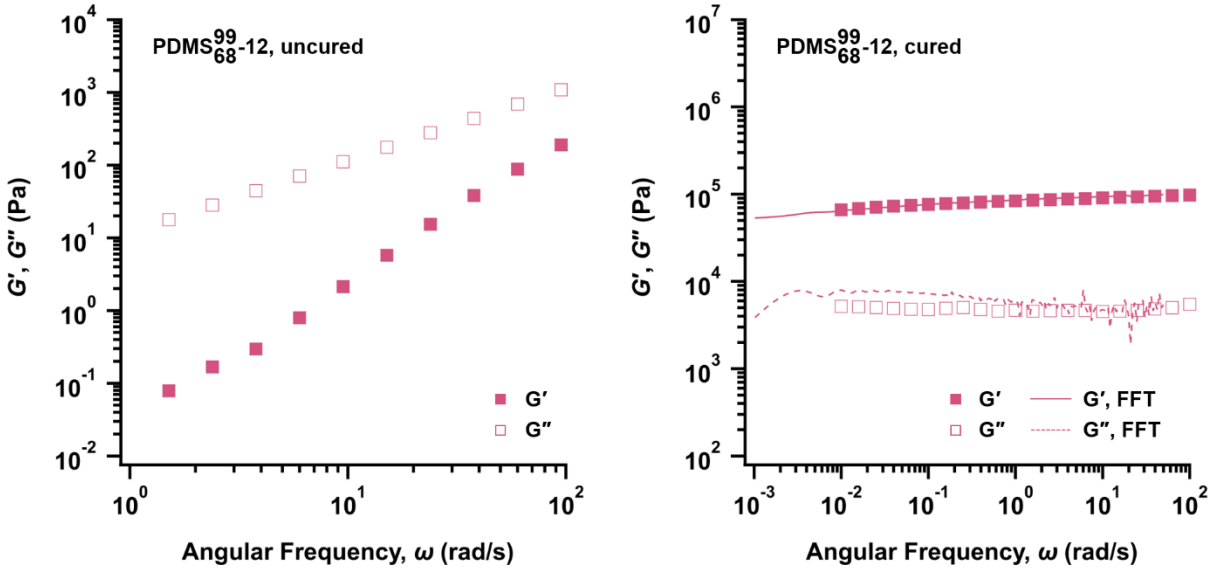

Figure S9. Frequency dependence of the shear moduli for uncured PDMS$_{68}^{99}$-12 at 21 ºC with an oscillatory strain amplitude of 0.05 (left) and for crosslinked PDMS$_{68}^{99}$-12 at 21 ºC with an oscillatory strain amplitude of 0.01 after complete UV curing (right). The stress relaxation

response with a step strain of 0.01 was fast Fourier transformed (FFT) to extend the frequency range to 0.001 rad/s.

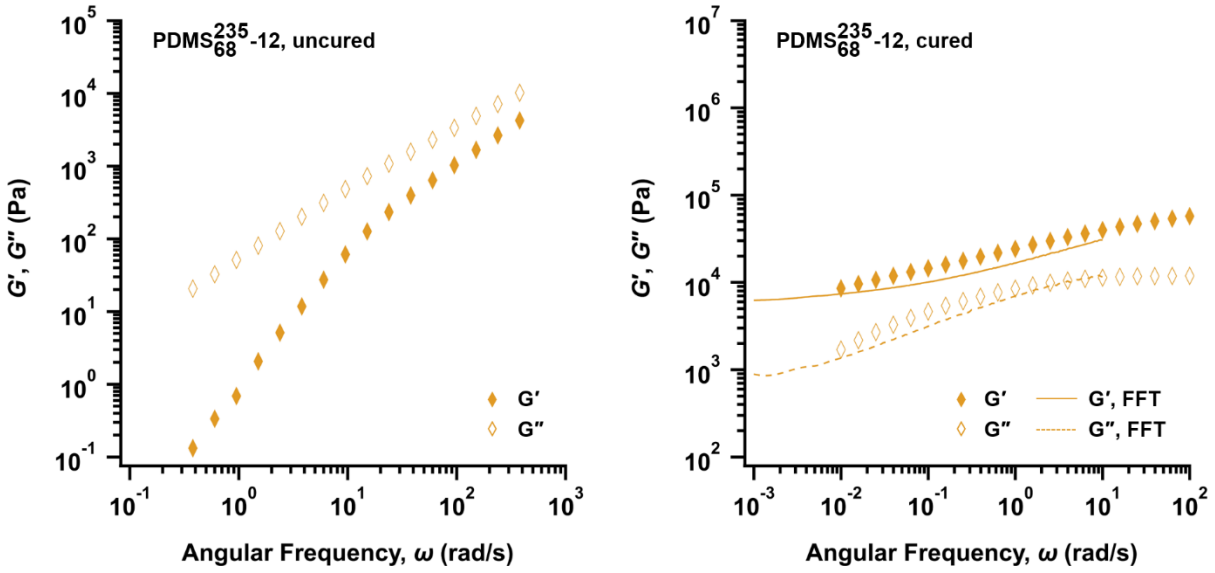

Figure S10. Frequency dependence of the shear moduli for uncured PDMS$_{68}^{235}$-12 at 21 ºC with an oscillatory strain amplitude of 0.05 (left) and for crosslinked PDMS$_{68}^{235}$-12 at 21 ºC with an oscillatory strain amplitude of 0.01 after complete UV curing (right). The stress relaxation response with a step strain of 0.01 was fast Fourier transformed (FFT) to extend the frequency range to 0.001 rad/s.

III. Dielectric and Optical Characterization

Dielectric Constant by Impedance Spectroscopy

The dielectric constants of a representative PDMS bottlebrush (PDMS$_{68}^{131}$-12) and Sylgard 184 were measured in the range of 100 Hz – 100 kHz with a 1 V amplitude using a Solartron 1260 Frequency Response Analyzer and 12962A room temperature sample holder. Figure S11 shows that the dielectric constant of the PDMS bottlebrush is 2.6 over the frequency range measured, matching that of Sylgard 184.

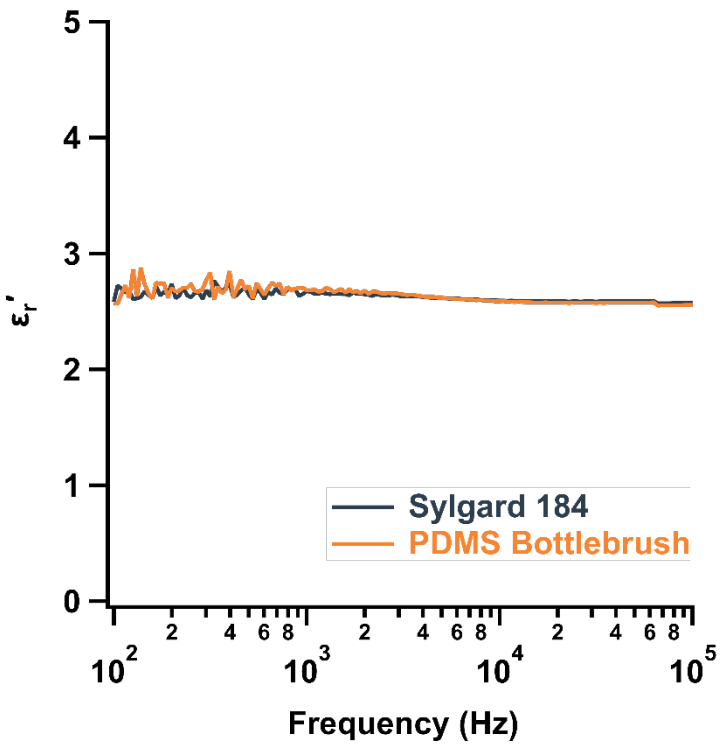

Figure S11. The frequency-dependent dielectric constant of a representative PDMS bottlebrush closely matches that of Sylgard 184.

Transmittance and Haze by UV-Vis Spectroscopy

The transmittance and haze of ITO-coated PET film (electrode material) and a sensor stack prepared with a representative PDMS bottlebrush ($PDMS_{68}^{20}$-2) were measured using a Shimadzu UV-3600 Spectrophotometer with an integrating sphere. Figure S12 shows that the transmittance and haze spectra of the sensor stack are closely matched with that of the ITO-coated PET film alone. The sensor has extremely low haze, < 1% over most of the visible spectrum.

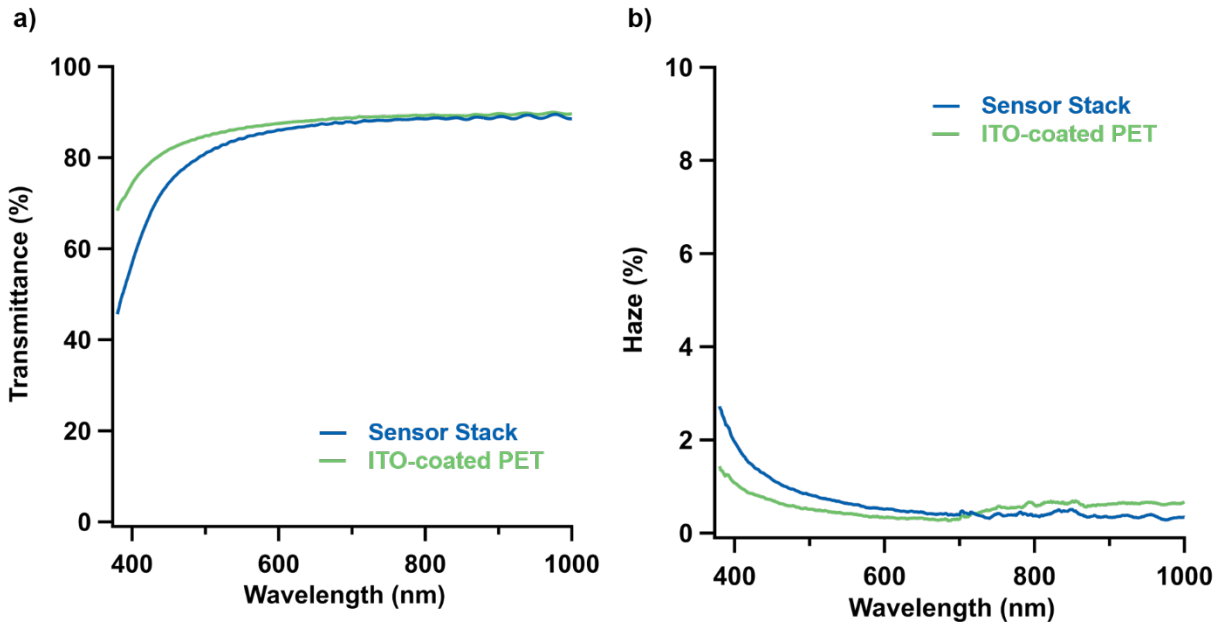

Figure S12. a) Transmittance spectra of ITO-coated PET film and a full sensor stack (two ITO-coated PET electrodes sandwiching a 0.2 mm PDMS bottlebrush film, $PDMS_{68}^{20}$-2). **b)** haze spectra of the same two samples.

Haze, defined as the ratio of diffuse transmittance, T_d, to total transmittance, T_t, was calculated using the following equations from ASTM D1003–13:[2]

$$T_t = \frac{T_2}{T_1}$$

$$T_d = \frac{1}{T_1}\left[T_4 - T_3\left(\frac{T_2}{T_1}\right)\right]$$

$$\text{Haze (\%)} = 100 \times \frac{T_d}{T_t}$$

In the above equations, T_1 represents the incident light transmitted without the sample in position, T_2 represents the total light transmitted by the sample, T_3 represents the light scattered by the instrument, and T_4 represents the light scattered by the instrument and sample.

IV. Relationship Between Elastomer Modulus and Device Sensitivity

Dielectric Elastomer Between Stretchable Electrodes:

The sensor geometry implemented in this work can be simply described as a parallel plate capacitor with capacitance C given as a function of dielectric permittivity $\varepsilon_0\varepsilon_\mathrm{r}$, electrode area A, and dielectric thickness d:

$$C = \frac{\varepsilon_0\varepsilon_\mathrm{r}A}{d}$$

Assuming elastomer incompressibility (Poisson's ratio, $\nu = 0.5$), deformation of the elastomer disc in uniaxial compression can be described by the following equations for extension ratios λ (z-direction, normal to the disc face; compression) and λ' (x and y directions, in the plane of the disc face; extension):

$$\lambda = \frac{d}{d_0}$$

$$\lambda\lambda'^2 = 1$$

$$\lambda' = \frac{1}{\sqrt{\lambda}}$$

$$A = \frac{A_0}{\lambda}$$

where A_0, d_0 are defined before deformation and A, d after deformation. Combining the above equations gives the relative change in capacitance ($\Delta C/C_0$) in terms of the disc normal extension ratio λ:

$$\frac{\Delta C}{C_0} = \frac{\frac{A}{d} - \frac{A_0}{d_0}}{\frac{A_0}{d_0}}$$

$$\frac{\Delta C}{C_0} = \lambda^{-2} - 1$$

The sensitivity of the sensor is defined as the relative change in capacitance divided by the applied compressive stress σ:

$$S = \frac{\frac{\Delta C}{C_0}}{\sigma} = \frac{\lambda^{-2} - 1}{\sigma}$$

Applying the network theory of rubber elasticity,[3] the final relationship between sensitivity S, shear modulus G, and extension ratio λ is:

$$\sigma = -G\left(\lambda - \frac{1}{\lambda^2}\right)$$

$$S = \frac{1}{G[\lambda + (\lambda + 1)^{-1}]}$$

Small strain limit: $\lambda \approx 1$, $S = \frac{2}{3G}$

Dielectric Elastomer between Rigid Electrodes (Constant Area Assumption):

A similar relationship can be derived for the case of rigid electrodes (capacitive response limited to that of the thickness change):

$$\frac{\Delta C}{C_0} = \frac{\frac{1}{d} - \frac{1}{d_0}}{\frac{1}{d_0}} = \frac{d_0}{d} - 1 = \lambda^{-1} - 1$$

$$S = \frac{1}{G(\lambda + \lambda^{-1} + 1)}$$

Small strain limit, $\lambda \approx 1$: $S = \frac{1}{3G}$

Note that in the small strain limit, the sensitivity of a device with stretchable electrodes is predicted to be double that of a device with rigid electrodes.

V. Experimental Stress–Strain Data Compared to Rubber Elasticity Models

The experimental stress–strain curves for each sensor were compared to curves predicted by two different models — the network theory of rubber elasticity[3] and the bonded rubber model from Gent & Lindley[4] and Gent & Meinecke[5] (to account for the effects of elastomer adhesion to the rigid electrodes). The three highest modulus elastomers showed behavior roughly tracking the network elasticity model while the curves for the two lowest modulus elastomers moved closer to that predicted by the bonded rubber model (Figure S13 and S14). Figure S15 shows the experiment stress–strain curves plotted together for reference.

(a) Network Theory of Rubber Elasticity[3]

$$\sigma = G\left(\lambda - \frac{1}{\lambda^2}\right)$$

(b) Compression of Bonded Rubber Blocks[4,5]

$$\sigma = \frac{E_a}{3}\left(\lambda - \frac{1}{\lambda^2}\right)$$

$$E_a = 3G\left(1 + \frac{r^2}{2d_0^2}\right)$$

$$\sigma = G\left(1 + \frac{r^2}{2d_0^2}\right)\left(\lambda - \frac{1}{\lambda^2}\right)$$

r = disc radius

d_0 = initial disc thickness

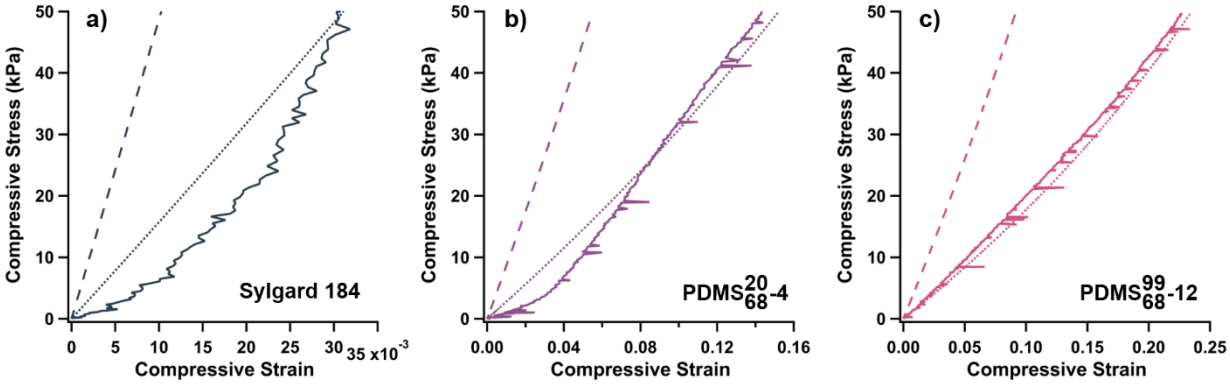

Figure S13. Stress-strain curves for the **a)** Sylgard 184, **b)** PDMS$_{68}^{20}$-4, and **c)** PDMS$_{68}^{99}$-12 sensors (solid lines) compared to theoretical curves predicted by the network theory of rubber elasticity (dotted lines) and the bonded rubber model (dashed lines). These three highest modulus conditions are roughly captured by the network theory of rubber elasticity.

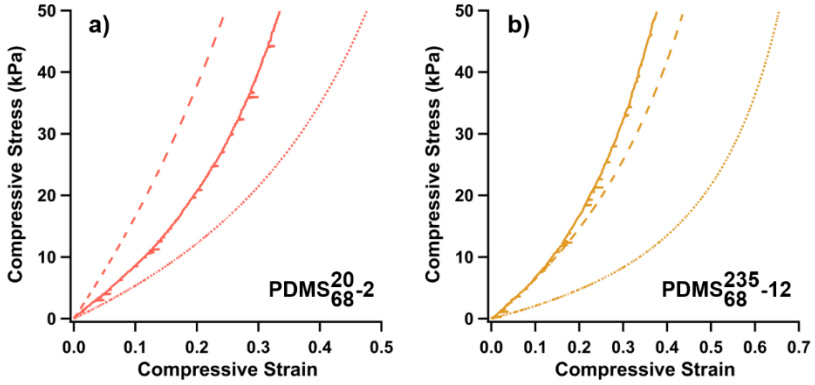

Figure S14. Stress-strain curves for the **a)** PDMS$_{68}^{20}$-2 and **b)** PDMS$_{68}^{235}$-12 sensors (solid lines) compared to theoretical curves predicted by the network theory of rubber elasticity (dotted lines) and the bonded rubber model (dashed lines). These two lowest modulus conditions show evidence of the influence of elastomer adhesion to the electrodes.

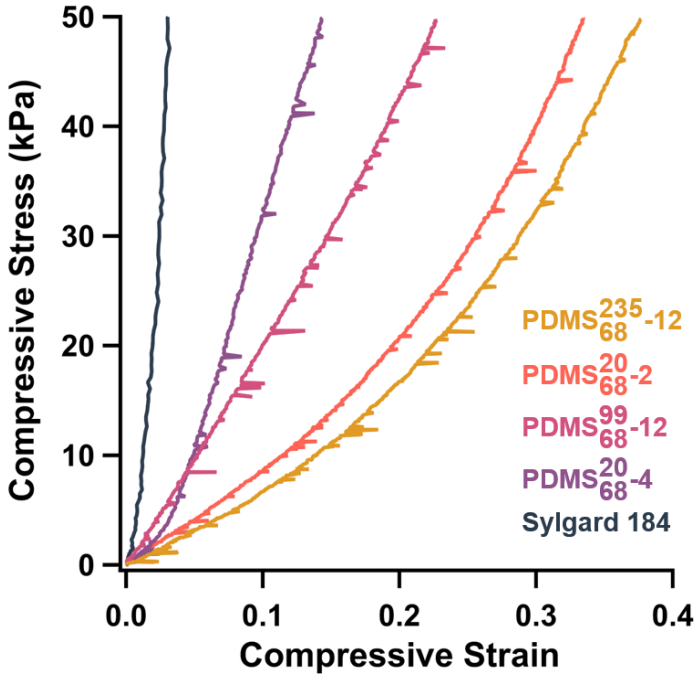

Figure S15. Stress–strain curves for the sensors tested.

VI. Table of Sensitivity Data for Elastomer-Based CPSs from Literature

Table S2. Sensitivity Data for Elastomer-Based CPSs from Literature

Elastomer Technology	Electrodes	Pressure Range (kPa)	Sensitivity (kPa^{-1})	$S/S_{control}$	Reference
Microporous Elastomer					
Prepared by sacrificial particle dispersion:					
Ecoflex + sugar granules, 44% porosity	Conductive fabric	0–100	0.0121	5.3	Atalay et al. (2018)[6]
Ecoflex + sugar cube, 63% porosity	CNT-Ecoflex composite	0–5 30–120	0.601 0.077	38 4.8	Kwon et al. (2016)[7]
Sylgard 184 + sugar granules, 89% porosity	ITO-coated PET	0–10 10–100	0.51285 0.01097	8.2 1.3	Yoon et al. (2017)[8]
Sylgard 184 + 6 μm poly(styrene) beads	ITO-coated PET	0–1	0.63	7.9	Kang et al. (2016)[9]
Prepared by water droplet dispersion:					
Sylgard 184 + 30 w% dispersed water	ITO-coated PET	0–0.1	0.8	4.0	Lee et al. (2016)[10]
Micropatterned Elastomer					
Sylgard 184, 6 μm pyrimidal features	ITO-coated PET	0–2 2–7	0.55 0.15	28 7.5	Mannsfeld et al. (2010)[11]
Polyurethane nano-needles	Aluminum foil	0–1 1–6	1.76 0.0268	17 1.1	Kim et al. (2012)[12]
Bulk Bottlebrush Elastomer					
PDMS Bottlebrush Elastomers	ITO-coated PET	0–10 20–50	0.0087 0.0053	22 53	This work

VII. Step Compression Examples

Step compressions of 1 kPa and 10 kPa were applied to the $PDMS_{68}^{99}$-12 and $PDMS_{68}^{235}$-12 sensors using a TA Instruments DMA 850. As expected from rheology studies, the $PDMS_{68}^{99}$-12 sensor exhibits more rapid response times than the $PDMS_{68}^{235}$-12 sensor (Figure S16).

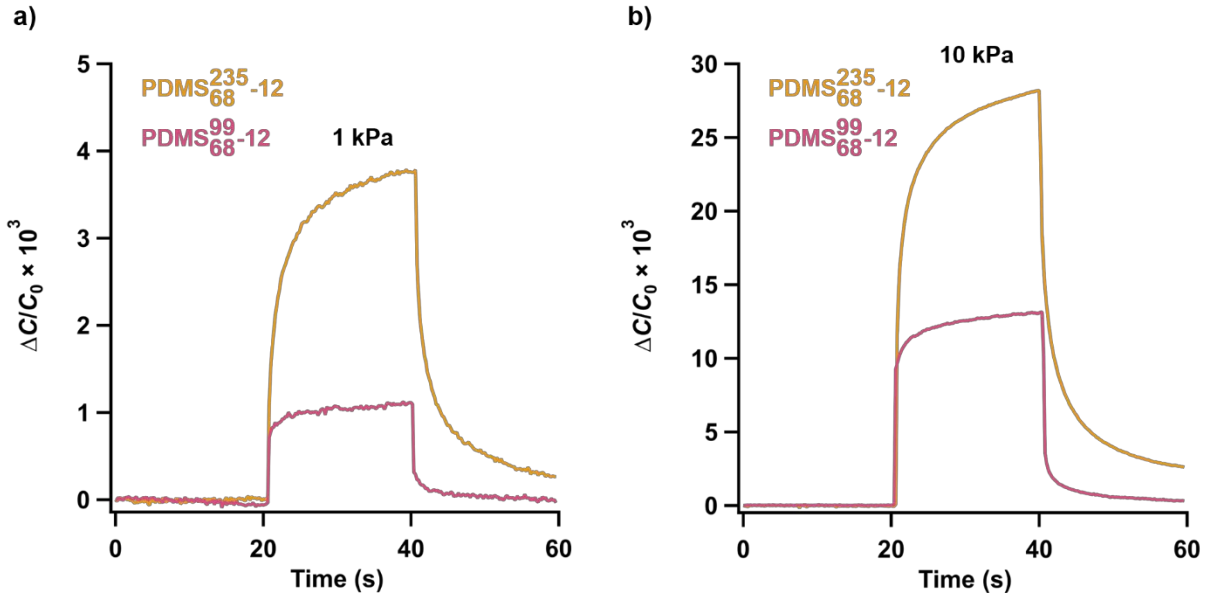

Figure S16. Sensor response to step compressions of **a)** 1 kPa, and **b)** 10 kPa.

VIII. Sensor Flexibility Demonstration

To demonstrate the mechanical flexibility of the sensor, a fixture was designed to apply compressive strain in a bent configuration (see inset of Figure S17; curvature $\kappa = 0.55$ cm^{-1}). The response curve of a representative PDMS bottlebrush elastomer sensor (prepared with $PDMS_{68}^{131}$-12; 12.7 mm diameter electrodes and elastomer) was measured using the strain-controlled test set-up with a 44 N load cell (Figure S17). The bent configuration applies a gradient pre-strain with a point of zero strain in the middle of the layer.

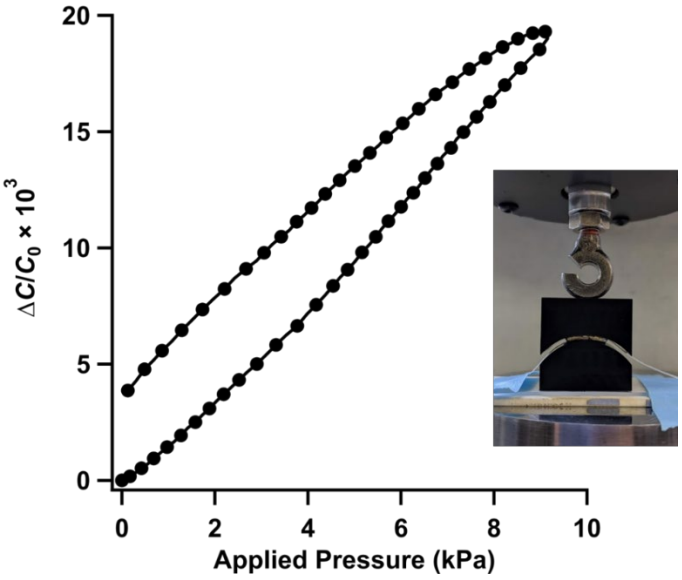

Figure S17. Sensor response curve for a bottlebrush elastomer CPS in a bent configuration.

References:

1 M. Tassieri, M. Laurati, D. J. Curtis, D. W. Auhl, S. Coppola, A. Scalfati, K. Hawkins, P. R. Williams and J. M. Cooper, *J. Rheol. (N. Y. N. Y).*, 2016, **60**, 649–660.

2 Standard Test Method for Haze and Luminous Transmittance of Transparent Plastics, https://www.astm.org/Standards/D1003.htm.

3 L. R. G. Treloar, *The Physics of Rubber Elasticity*, Oxford University Press, New York, 3rd edn., 1975.

4 A. N. Gent and P. B. Lindley, *Proc. Inst. Mech. Eng.*, 1959, **173**, 111–122.

5 A. N. Gent and E. A. Meinecke, *Polym. Eng. Sci.*, 1970, **10**, 48–53.

6 O. Atalay, A. Atalay, J. Gafford and C. Walsh, *Adv. Mater. Technol.*, 2018, **3**, 1700237.

7 D. Kwon, T. I. Lee, J. Shim, S. Ryu, M. S. Kim, S. Kim, T. S. Kim and I. Park, *ACS Appl. Mater. Interfaces*, 2016, **8**, 16922–16931.

8 J. Il Yoon, K. S. Choi and S. P. Chang, *Microelectron. Eng.*, 2017, **179**, 60–66.

9 S. Kang, J. Lee, S. Lee, S. G. Kim, J. K. Kim, H. Algadi, S. Al-Sayari, D. E. Kim, D. E. Kim and T. Lee, *Adv. Electron. Mater.*, 2016, **2**, 1600356.

10 B. Y. Lee, J. Kim, H. Kim, C. Kim and S. D. Lee, *Sensors Actuators, A Phys.*, 2016, **240**, 103–109.

11 S. C. B. Mannsfeld, B. C. K. Tee, R. M. Stoltenberg, C. V. H. H. Chen, S. Barman, B. V. O. Muir, A. N. Sokolov, C. Reese and Z. Bao, *Nat. Mater.*, 2010, **9**, 859–864.

12 J. Kim, T. Nga Ng and W. Soo Kim, *Appl. Phys. Lett.*, 2012, **101**, 103308.